Original Research

Chromobox 4 facilitates tumorigenesis of lung adenocarcinoma through the Wnt/β-catenin pathway

Zuoyun Wang [a,b,c]; Zhaoyuan Fang [a,b,c]; Gaobin Chen [a,b,c]; Bo Liu [d]; Jinjin Xu [a,b,c]; Fei Li [a,b,c]; Fuming Li [a,b,c]; Hongyan Liu [a,b,c]; Haoen Zhang [a,b,c]; Yihua Sun [e]; Gang Tian [f]; Haiquan Chen [e]; Guoliang Xu [b,c]; Lei Zhang [a,b,c,f]; Liang Hu [a,b,c,*]; Hongbin Ji [a,b,c,f,*]

[a] State Key Laboratory of Cell Biology, Chinese Academy of Sciences, Shanghai, China
[b] Shanghai Institute of Biochemistry and Cell Biology, Chinese Academy of Sciences, Shanghai, China
[c] Center for Excellence in Molecular Cell Science, Chinese Academy of Sciences, Shanghai, China
[d] CAS Key Laboratory of Molecular Virology and Immunology, Institute Pasteur of Shanghai, Chinese Academy of Sciences, Shanghai, China
[e] Department of Thoracic Surgery, Fudan University Shanghai Cancer Center, Fudan University, Shanghai, China
[f] School of Life Science and Technology, Shanghai Tech University, Shanghai, China

Abstract

Chromobox 4 (CBX4) is a core component of polycomb-repressive complex 1 with important roles in cancer biology and tissue homeostasis. Aberrant expression of CBX4 has been implicated in several human malignancies. However, its role and underlying mechanisms in the tumorigenesis of lung adenocarcinoma (LUAD) have not been defined in vivo. Here, we found that expression of CBX4 was frequently up-regulated in human LUAD samples and correlated with poor patient survival. Importantly, genetic ablation of CBX4 greatly dampened lung tumor formation and improved survival in the $Kras^{G12D}$/$P53^{L/L}$ (KP) autochthonous mouse model of LUAD. In addition, CBX4 depletion significantly inhibited proliferation and anchorage-independent growth of KP mouse embryonic fibroblasts. Moreover, ectopic CBX4 expression clearly promoted proliferation and anchorage-independent growth in both human and mouse LUAD cells, whereas silencing of CBX4 exerted opposite effects. Mechanistically, CBX4 promoted growth of LUAD cells through activation of the Wnt/β-catenin pathway. Furthermore, expression levels of CBX4 were positively correlated with β-catenin in human LUAD samples. In conclusion, our data suggest that CBX4 plays an oncogenic role via the Wnt/β-catenin pathway and could serve as a potential therapeutic target in LUAD.

* Corresponding authors.
E-mail addresses: liang.hu@sibcb.ac.cn (L. Hu), hbji@sibcb.ac.cn (H. Ji).

Introduction

Lung cancer is one of the leading causes of cancer-related death worldwide. Among the primary lung cancers, lung adenocarcinoma (LUAD) represents the most frequent histologic subtype. Despite recent advancements in new interventions such as targeted therapies and immunotherapy, the overall survival of patients with LUAD remains at a very low level [1–3]. Great efforts have been made to explore the mechanism underlying the pathogenesis of LUAD during the past decades; however, the detailed molecular events that contribute to LUAD development and progression are still not fully understood. Therefore, it is urgently need to search for novel therapeutic targets for LUAD therapy.

Polycomb group (PcG) proteins are known as master transcriptional repressors that form 2 dominant polycomb-repressive complexes (PRC), PRC1 and PRC2. PcG proteins epigenetically modify chromatin to control multiple physiological processes including stem cell self-renewal, DNA repair, differentiation and senescence [4–8]. Growing evidence has revealed that PcG proteins link to tumorigenesis, and serve as biomarkers for prognosis and therapeutic response and also attractive targets for tumor intervention [9]. For instance, pharmacologic inhibition of EZH2, the catalytic subunit of PRC2, has been demonstrated to be a promising treatment in various types of cancer including lung cancer [10–15]. Thus, exploring the roles of PcG proteins in the development of LUAD may facilitate the discovery of new prognostic biomarkers and potential therapeutic targets for patients with LUAD.

As core components of PRC1, chromobox (CBX) family proteins are involved in mediating the recruitment and stabilization of PRC1 to target chromatin [16,17]. Though structural similarities and functional redundancies are reported among CBX proteins, different members of CBX family, such as CBX2, CBX7, and CBX8, have been documented to function either as oncogenes or tumor suppressors in a cancer type-dependent manner [18–24]. Up-regulation of CBX2 is observed in multiple cancer types that predicts aggressive progression and worse overall survival [19]. CBX7 exhibits tumor suppressor activity in thyroid, colon, and lung cancers, whereas plays an oncogenic role in the gastric cancer [25]. CBX4 is a unique CBX family member with respect to its E3 SUMO-protein ligase activity [26,27]. It has been revealed that CBX4 promotes liver tumor angiogenesis through HIF-α sumoylation and is an unfavorable prognostic factor for patients with hepatocellular carcinoma [27]. CBX4 has the ability to impair tumor metastasis via suppression of Runx2 expression through recruitment of HDAC3 in colorectal carcinoma [28]. These findings indicate that the role of CBX4 is tissue-dependent and varies with the type of malignancy. Using established human lung cancer cell lines, Hu et al recently reported that CBX4 promotes the proliferation and metastasis in lung cancer [29], supporting a cancer-promoting role for CBX4 in lung cancer. While given the significant differences among distinct histologic subtypes of lung cancer and between cell model-based and animal model-based in vivo studies, whether CBX4 plays a role in the initiation and development of autochthonous LUAD tumors in vivo has yet to be determined.

In the present study, we evaluated the expression status and clinical relevance of CBX4 in LUAD patients. In addition, we comprehensively analyzed the effects of CBX4 in a well-established autochthonous genetically engineered mouse model (GEMM) of LUAD, and mouse embryonic fibroblasts (MEFs) as well as human and mouse LUAD cells. We further explored the mechanism of action of CBX4, which might shed a new light on the pathogenesis of LUAD.

Methods

Mouse cohorts and treatment

The $Kras^{G12D}$ and $P53^{L/L}$ mice were originally generously provided by Dr. Tyler Jacks, Dr. Kwok-Kin Wong, and Dr. Ronald A. DePinho, respectively. $Cbx4^{L/L}$ mice were generated and genotyped as described previously [30]. All mice were housed in a specific pathogen-free environment at the Shanghai Institute of Biochemistry and Cell Biology and treated in strict accordance with protocols approved by the Institutional Animal Use Committee of the Shanghai Institutes for Biological Sciences, Chinese Academy of Sciences. At an age of 8 weeks, $Kras^{G12D}/P53^{L/L}$ (KP) and $Kras^{G12D}/P53^{L/L}/Cbx4^{L/L}$ (KPC) mice were treated with 2×10^6 PFU Adeno-Cre by nasal inhalation as previously described [31]. All mice were sacrificed for gross inspection and pathologic examination. Lung tumors were dissected for molecular analyses. Mice lung tissues were inflated and fixed in 4% formalin, embedded in paraffin and sectioned for hematoxylin and eosin (H&E) staining. Tumor

count was evaluated by microscopy and tumor size was analyzed using the Image-J software.

Plasmids

hCBX4 and mCbx4 expressing plasmids were cloned into the lentivirus based vector pCDH-CMV-MCS-EF1 vector. Human ShCBX4s knockdown plasmids were cloned into the MLP vector and mouse ShCBX4s knockdown plasmids were cloned into the pLKO.1 vector.

Cell culture and viral infection

We generated MEFs from 13.5 postcoitum embryos and grew them in DMEM medium containing 10% fetal bovine serum (FBS), 100 μg/mL streptomycin and 100 mg/mL penicillin. The MEFs were then cultured for at least 2 more passages before cells were used for various functional assays. Human lung LUAD cell lines, HEK-293T, MEFs, and KP mouse LUAD cells were cultured in DMEM containing 10% FBS. Lentiviral infection was done as follows: HEK-293T cells were co-transfected with MLP, pLKO.1 or pCDH constructs and packaging plasmids. The progeny viruses released from HEK-293T cells were filtered, collected, and used to infect A549, NCI-H1299, NCI-H358, KP mouse LUAD cells, and MEFs.

Fluorescence Activating Cell Sorter (FACS) assay

For cell cycle analysis, virus-infected cells were harvested at 80% confluency and fixed with 75% ethanol. Then the cells were taken for propidium iodine (PI) staining and cell cycle was analyzed using flow cytometry.

3-(4,5-Dimethylthiazol-2-yl)-2,5-diphenyltetrazolium bromide (MTT) assay

For the MTT assay, virus-infected cells were seeded in 96-well plate and the viability of cells was measured daily for 5 d. Briefly, 20 μL of MTT working solution (5 mg/mL) was added into each well and incubated at 37°C for 4 h. Then the supernatants were removed and the resultant MTT formazan was dissolved in 100 μL of dimethyl sulfoxide (DMSO). The absorbance was measured at the wavelengths of 570 nm and 630 nm.

Soft agar assay

For soft agar colony formation assay, 3000 or 5000 virus-infected cells were resuspended in their respective growth medium containing an additional 0.2% agar and layered onto 1% agar beds in 6-well plates. Culture medium was changed every 3 d for 4 wk before subjected to 0.005% crystal violet staining. The number of colonies was evaluated by microscopy.

Real-time polymerase chain reaction (PCR) assay

RNA was extracted using Trizol (Invitrogen) following the manufacturer's instruction. RNA samples were reverse transcribed using Revert Aid First Strand cDNA Synthesis Kit (Fermentas). Genomic DNA from mice was extracted using Gentra Puregene Tissue Kit (Qiagen). cDNA was subjected to quantitative real-time PCR with gene-specific primers using the 7500 Fast Real-Time PCR System (Applied Biosystems) and the SYBR Green Master PCR mix (Invitrogen). Actin was served as an internal control. Primers used in this study were listed in Table S1.

Western blot analysis

Total protein lysate were prepared by homogenization in protein loading buffer. Equal amounts of protein were separated by electrophoresis on an SDS-PAGE gel and transferred onto PVDF membranes. Western blot analysis was performed using the following antibodies: CBX4 from Santa Cruz (1:500, SC-199929); β-catenin from Proteintech (1:1000, 51067-2-AP); c-MYC from Abclonal (1:1000, A17332); CyclinD1 from CST (1:1000, #2926); Tublin from DSHB (1:1000, E7); and Actin from Sigma-Aldrich (1:1000, A1978).

RNA interference

Human β-catenin small interference RNA (siRNA) and the control siRNA were obtained from Shanghai GenePharma, Co., Ltd., Shanghai, China. siRNA oligonucleotides were transfected in A549 by Lipofectamine RNAi MAX (Invitrogen) following the manufacturer's instructions. Two pairs of siRNAs were used to perform experiments. siRNAs used in this study are listed below:

siβ-catenin 1: 5′-CCCUAGCCUUGCUUGUUAATT-3′;
siβ-catenin 2: 5′-GGGUAAAUCAGUAAGAGGUTT-3′;
si KRAS 1: 5′-CCUUGACGAUACAGCUAAUTT-3′;
si KRAS 2: 5′-GGAUUCCUACAGGAAGCAATT-3′.

The scramble siRNA was used as control siRNA. The control siRNA sequence is: 5′-UUCUCCGAACGUGUCACGUTT-3′.

Immunofluorescence staining analysis

Cells were fixed in 4% formaldehyde in phosphate-buffered saline (PBS) buffer at room temperature for 10 min, washed with PBS buffer, and then treated with PBST (PBS and 0.25% Triton X-100) for permeabilization. Cells or frozen sections were blocked with PBSA (PBS and 3% BSA) for 30 min and incubated with primary antibody overnight in PBSA at 4°C. Primary antibodies used in this study were: KI67 (1:300, SC-23900); β-catenin (1:100, Proteintech-51067-2-AP). Cells were then washed with PBST and incubated with secondary antibody diluted in PBSA for 1 h at room temperature. Secondary antibodies used were Alexa Fluor 552 conjugated goat anti-rabbit a dilution of 1:1000. DAPI was used to stain the nuclei. Samples were mounted with Aqua-Poly/Mount (Polysciences). For analysis of the KI67 staining, at least 10 fields were counted.

Immunohistochemistry analysis

Immunohistochemistry (IHC) was performed as described previously [32]. Briefly, slides were deparaffinized in xylene and rehydrated sequentially in ethanol. Slides were quenched in hydrogen peroxide (0.3%–3%) to block endogenous peroxidase activity and then washed in PBS. And then the slides were blocked in 5% normal murine serum for 30 min at 37°C temperature. Slides were then incubated overnight at 4°C with primary antibody diluted in blocking buffer. The avidin-biotin peroxidase complex method was used and then the slides were counterstained with hematoxylin. The proliferation rate was evaluated by counting KI67-positive nuclei following staining at high-power field for more than 30 fields for each group and the method was conducted as previously described [33]. For IHC staining, the stained sections were evaluated in a blinded manner without prior knowledge of the clinical information using the German immunoreactive score (IRS) as described previously [32,34]. Briefly, the IRS was assigned considering both the intensity of staining and the proportion of tumor cells with positive staining. The intensity was scored as follows: no staining = 0; weak staining = 1; moderate staining = 2; strong staining = 3. The extent

of stained cells: <5% = 0; 5%–25% = 1; 25%–50% = 2; 50%–75% = 3; 75%–100% = 4. The final IRS was determined by multiplying the intensity and extent of positivity score of stained cells, with the minimum score of 0 and a maximum score of 12. CBX4 antibody for IHC was generated by Dr. Guoliang Xu and described previously [30]; KI67 (1:1000, SC-23900); Cleaved caspase-3 (1:200, CST #9661); β-catenin (1:2000, Proteintech-51067-2-AP); and VEGFR2 (CST #55B11).

Human LUAD samples analysis

A total of 72 pathologically confirmed human LUAD specimens and 7 normal lung specimens were collected in Fudan University Shanghai Cancer Center between January 2008 and December 2009 with written consents of patients and the approval from the Institute Research Ethics Committee. All tumor specimens were taken at the time of surgical resection. Survival analyses of 72 LUAD patients in the study cohort were performed based on CBX4 protein expression status using the Kaplan-Meier plotter analysis. The median IRS value (IRS = 4) of intratumoral CBX4 expression was chosen as the cut-off for differentiating between high and low CBX4 expression. An IRS of $\geq$4 was used to define tumors with high CBX4 expression and an IRS of <4 was used to indicate tumors with low CBX4 expression. In addition, the prognostic significance of CBX4 expression was further evaluated based on CBX4 mRNA expression status in publicly available human LUAD datasets containing 719 patients using an online Kaplan-Meier plotter analysis tool (http://www.kmplot.com/lung) [35]. Patients were also divided into high and low CBX4 expression subgroups with its median expression value as the cut-off.

Statistical analysis

Data were presented as mean $\pm$ standard error of the mean unless otherwise indicated. Differences was determined using the Student's t test or 1-way analysis of variance (2-sided) in multiple groups, with the Tukey-Kramer multiple comparison test for post hoc comparisons. Kaplan-Meier analysis with log-rank test was used to assess patients' survival between subgroups. Spearman correlation analysis was used to evaluate the correlation between CBX4 and β-catenin expression in human LUAD. All statistical analyses were carried out using GraphPad Prism 5 software, and P value <0.05 was considered to be statistically significant.

Results

CBX4 expression is frequently up-regulated in human LUAD tissues and correlates with unfavorable prognosis

To determine the clinical relevance of CBX4 in LUAD, we first analyzed the mRNA levels of the CBX4 between paired LUAD tissues and adjacent normal lung counterparts using TGGA-LUAD datasets. CBX4 were significantly increased in cancerous tissues compared to adjacent normal tissues (Figure 1A). Real-time PCR analyses showed that most (8 out of 10) human LUAD samples harbored up-regulated CBX4 expression in comparison with normal lungs (Figure 1B). IHC analysis of 79 human tissue samples including 72 LUADs and 7 normal lungs further confirmed that levels of CBX4 protein were elevated in majority of the LUAD tissues relative to normal lung counterparts (Figure 1C,D). Importantly, survival analysis of the 72 LUAD patients revealed that patients with high intratumoral CBX4 expression had a significantly shorter survival time than those with low CBX4 expression (Figure 1E). We further evaluated the prognostic value of CBX4 expression in publicly available human LUAD datasets containing 719 patients using an online Kaplan-Meier plotter analysis tool (http://www.kmplot.com/lung) [35] and observed similar results (Figure 1F).
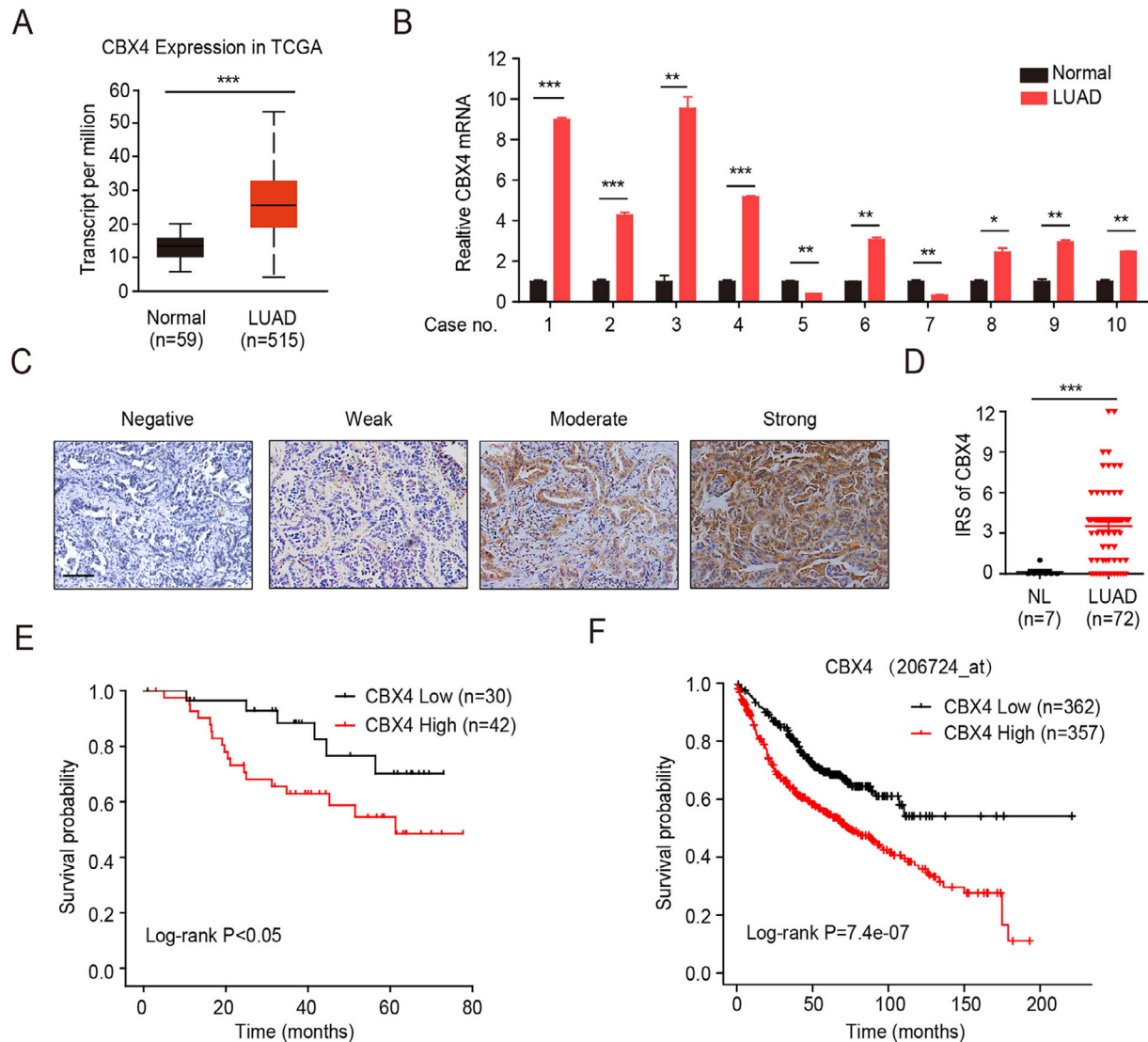
Fig. 1. CBX4 expression is frequently up-regulated in human LUAD tissues and correlates with unfavorable prognosis. (A) Lung cancer TGGA database analyses of the CBX4 mRNA expression in human in lung adenocarcinomas (LUAD) and normal lung (NL). (B) Real-time PCR analysis of the CBX4 mRNA expression in paired lung adenocarcinoma tissues and adjacent normal lung counterparts. (C) Representative IHC staining of CBX4 in LUAD samples. Scale bar: 100 μm. (D) Statistical analysis of CBX4 staining in human lung LUAD (N = 72) and NL samples (N = 7). (E) Kaplan-Meier curves for overall survival of the 72 LUAD patients in the study cohort according to CBX4 protein expression status. Patients were divided into high and low CBX4 expression subgroups with its median IRS value as the cut-off. (F) Kaplan-Meier curves for overall survival of 719 LUAD patients using a publicly available online Kaplan-Meier plotter analysis tool (http://www.kmplot.com/lung) according to CBX4 mRNA expression status. Patients were also divided into high and low CBX4 expression subgroups with its median expression value as the cut-off. Data are shown as means ± SEM. *$P < 0.05$, **$P < 0.01$, ***$P < 0.001$.

While, no significant survival difference were observed between high and low CBX4 expression in patients with lung squamous cell carcinoma (LUSC) (Figure S1). These data indicate the potential functional importance of CBX4 overexpression in LUAD.

Genetic ablation of CBX4 greatly dampens tumorigenesis and prolongs survival in the KP *autochthonous mouse model of LUAD*

The *Kras^{G12D}/P53$^{L/L}$* (*KP*) mouse model is a well-established autochthonous model for the study of LUAD tumorigenesis [36]. We then checked the protein levels of CBX4 in the primary tumors from *KP* model. Consistent with the findings from human LUAD samples, the protein levels of CBX4 were also increased in the cancerous tissues compared with adjacent normal tissues from *KP* mice (Figure 2A).

To determine the role of CBX4 in LUAD tumorigenesis in vivo, we crossed *Cbx4$^{L/L}$* mice with *KP* mice to generate the *Kras^{G12D}/P53$^{L/L}$/Cbx4$^{L/L}$* (*KPC*) mice. The resultant *KPC* or *KP* mice were administrated with Adeno-Cre through nasal inhalation to induce lung tumors as previously described (Figure 2B) [37]. Eight weeks post Ade-Cre treatment, multiple tumor nodules could easily be seen on the surface of the lungs of *KP* mice (Figure 2C). In contrast, only few tumor nodules could be observed on the surface of lungs of *KPC* mice (Figure 2C). Importantly, deletion of CBX4 significantly prolonged the survival of *KP* mice (median survival times: 16.9 weeks in *KPC* mice vs 8.3 weeks in *KP* mice, *P* < 0.001; Figure 2D). Histopathologic analysis showed that *KP* mice developed multiple cancerous lesions in the lungs at 8 weeks after Adeno-Cre treatment, whereas fewer and smaller cancerous lesions could be detected in the lungs of *KPC* mice (Figure 2E). Quantitative analysis confirmed that both tumor number and
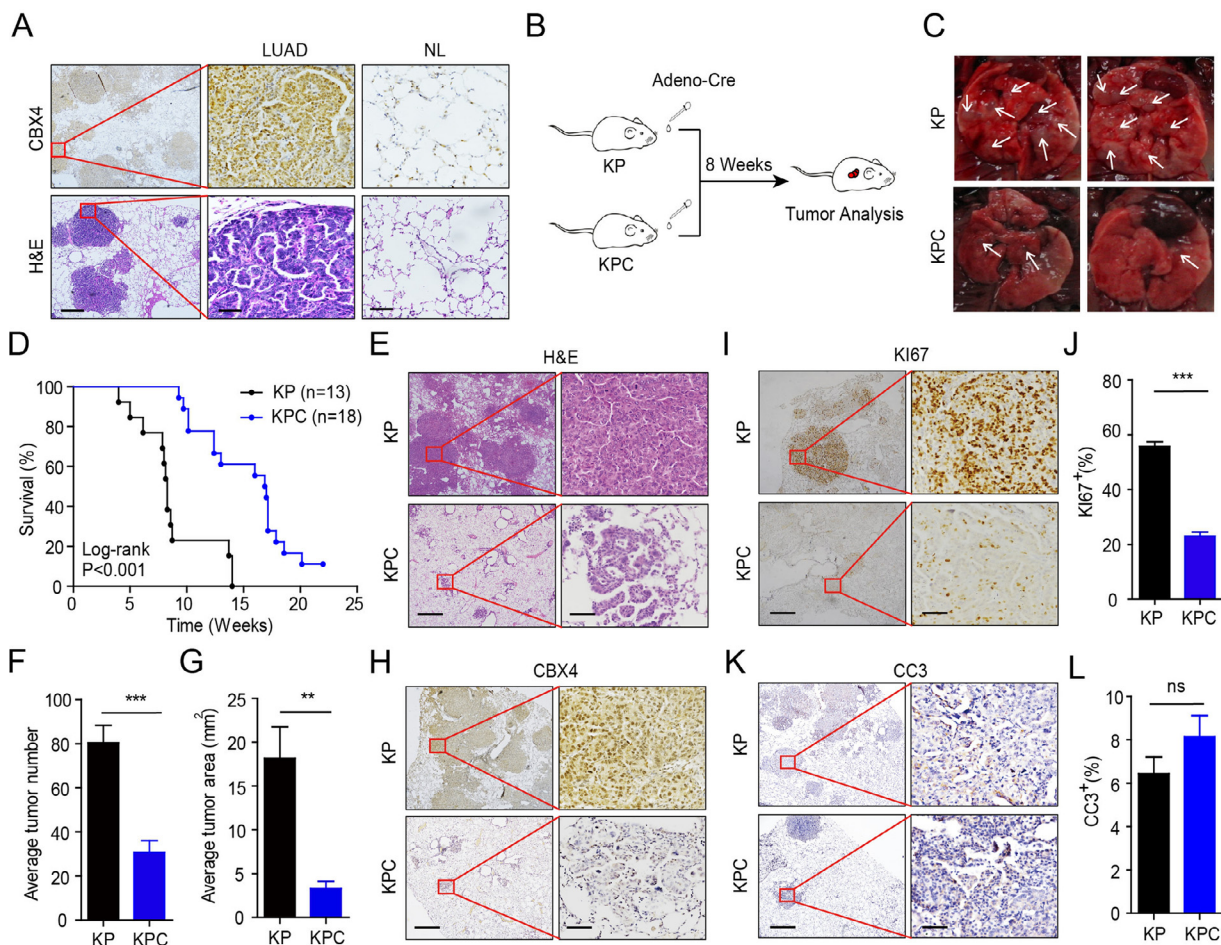
Fig. 2. Genetic deletion of CBX4 alleviates tumorigenesis and prolongs survival in the *KP* autochthonous mouse model of LUAD. (A) Representative IHC staining of CBX4 and H&E staining in lung sections from *KP* mice. Scale bar: 500 μm (left); 50 μm (middle and right). (B) A scheme for Adeno-Cre virus treatment in *KP* and *KPC* mouse model. (C) Representative photographs of lungs of *KP* and *KPC* mice after inhalation of Adeno-Cre at 8 wk. Arrows indicate tumor lesions. (D) Kaplan-Meier survival curves of the *KP* mice group (n = 13) and the *KPC* mice group (n = 18) after Adeno-Cre treatment. The *P* value was determined using the log-rank test. (E) Representative H&E staining in lung sections from *KP* and *KPC* mice. Scale bar: 500 μm (left); 50 μm (right). (F and G) Quantification of average tumor number per mouse (F) or tumor area per mouse (G) in lung sections from *KP* and *KPC* mice. (H) Representative IHC staining of CBX4 in lung sections from *KP* and *KPC* mice. Scale bar: 500 μm (left); 50 μm (right). (I) Representative IHC staining of KI67 in lung sections from *KP* and *KPC* mice. Scale bar: 500 μm (left); 50 μm (right). (J) Percentage of KI67 positive staining in lung tumors from *KP* and *KPC* mice. (K) Representative IHC staining of cleaved caspase-3 (CC3) in lung sections from *KP* and *KPC* mice. Scale bar: 500 μm (left); 50 μm (right). (L) Percentage of CC3 positive staining in lung tumors from *KP* and *KPC* mice. The percentage of KI67 and CC3 staining were quantified by counting 50 views in 4 mice per group. Data are shown as means ± SEM. **$P < 0.01$, ***$P < 0.001$.

the tumor area were dramatically reduced in *KPC* vs *KP* mice (Figure 2F,G). As expected, tumors from *KPC* mice barely expressed CBX4 (Figure 2H). Further IHC analysis revealed that deletion of CBX4 greatly suppressed the proliferation of cancer cells, as indicated by decreased Ki67 staining in *KPC* mice compared with *KP* mice (Figure 2I,J). While no substantial differences in the staining of cleaved caspase-3 (CC3), a marker of apoptosis, were observed between the 2 groups (Figure 2K,L). Thus, results from the autochthonous GEMM of LUAD strongly suggest an oncogenic role of CBX4 in the tumorigenesis of LUAD.

CBX4 is essential for anchorage-independent growth of KP *MEFs*

To further evaluate the oncogenic activity of CBX4, we generated MEFs from the *KP, KPC,* and wide-type (*WT*) mice. The MEFs were infected with Adeno-Cre to activate *Kras*^{G12D} with concurrent knockout *P53* and *Cbx4* at the genomic DNA level. Consistent with previous studies, *WT* MEFs quickly underwent senescence within a few passages, whereas *KP*

MEFs exhibited enhanced proliferative properties and developed resistance to cellular senescence [38]. Immunofluorescence staining analysis showed that *KP* MEFs had increased percentages of Ki67 positive cells compared with *WT* MEFs, which could be reduced following CBX4 depletion (Figure 3A,B). Cell cycle analysis revealed that *KP* MEFs had increased percentages of cells in S and G2/M phases compared with *WT* controls, which can be abrogated after CBX4 was deleted (Figure 3C,D). MTT assay showed that knockout of CBX4 suppressed the increased cell growth in *KP* MEFs (Figure 3E). Moreover, soft agar assay demonstrated that CBX4 deficiency profoundly inhibited the anchorage- independent growth in *KP* MEFs (Figure 3F,G). These data from MEFs experiments further confirm the oncogenic role of CBX4.

CBX4 exerts an oncogenic role in both human and mouse LUAD cells

To determine the roles of CBX4 in malignant phenotypes of LUAD cells in vitro, we checked the expression of CBX4 in multiple human LUAD cell
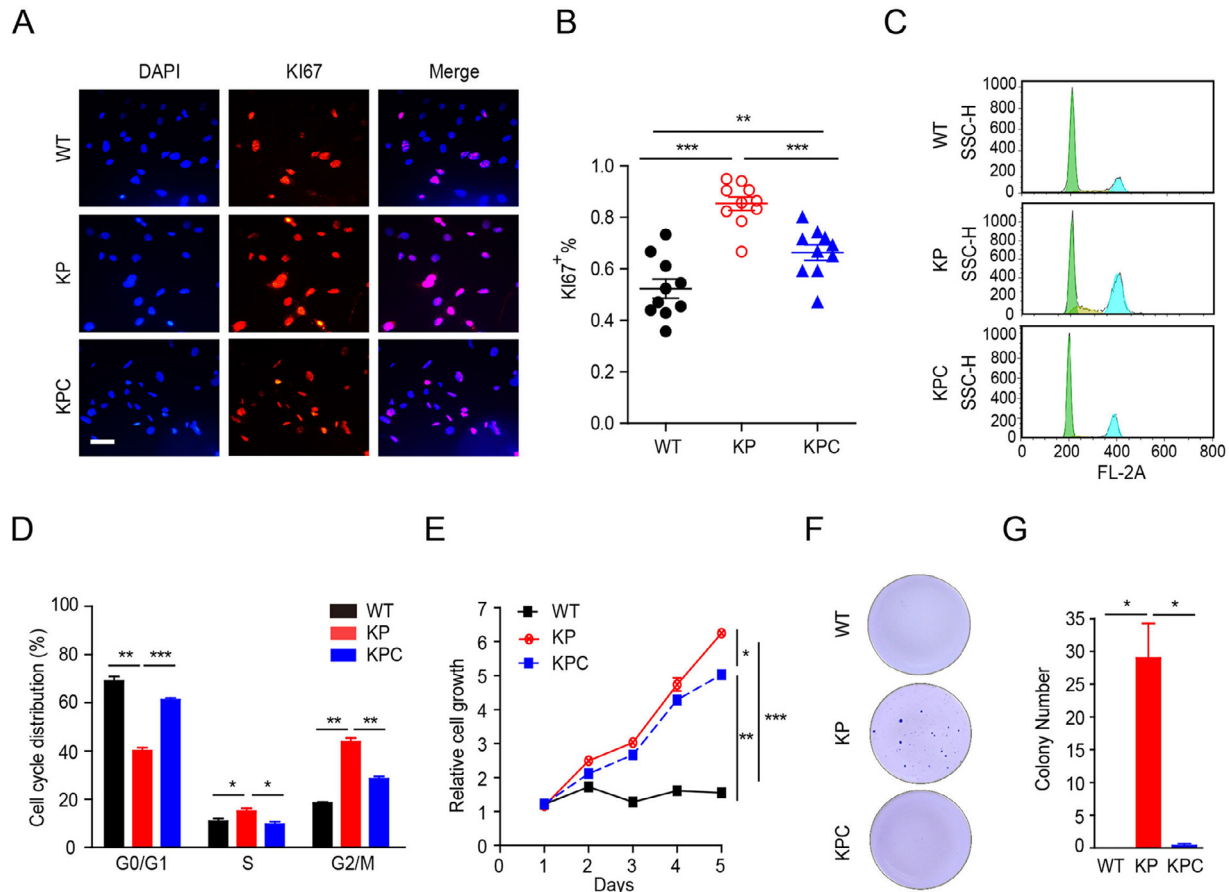
Fig. 3. CBX4 is essential for anchorage-independent growth of *KP* MEFs. (A) KI67 staining in *WT, KP,* and *KPC* MEFs. Scale bar: 500 μm. (B) Quantification of the KI67 staining in *WT, KP,* and *KPC* MEFs. (C and D) FACS assay of cell cycle distributions of MEFs isolated from the *WT, KP,* and *KPC* mice. (E) MTT analysis of cell proliferation in MEFs isolated from the *WT, KP,* and *KPC* mice. (F and G) Colony formation abilities of MEFs isolated from the *WT, KP,* and *KPC* mice were determined by soft agar assay. Data are shown as means $\pm$ SEM. *$P < 0.05$, **$P < 0.01$, ***$P < 0.001$, ns means no significance.

lines (Figure 4A). We constructed stable CBX4-overexpressed cell models in 2 human LUAD cell lines, A549 and NCI-H1299, which have relative middle or low levels of endogenous CBX4, respectively (Figure 4A–C). Consistently, ectopic expression of CBX4 promoted cell growth and also colony formation in soft agar in each cell line (Figure 4D–F). We also employed a *KP* tumor-derived cell line named L574, which was established previously by our lab [39], repeated these experiments and obtained similar results (Figure 4B–F). These findings indicate that CBX4 is sufficient to promote growth of LUAD cells.

To further determine the requirement of CBX4 in the malignant phenotypes of LUAD cells in vitro, we constructed stable CBX4-depleted cell models in A549 and NCI-H358, which have middle or high levels of endogenous CBX4 (Figure 4A), using 2 lentivirus-mediated shRNAs targeting CBX4. The knockdown efficiency was confirmed by real-time qPCR and western blot analysis (Figure 5A,B). Not surprisingly, knockdown of CBX4 resulted in reduced cell growth and soft agar colony formation capacity in both cell lines (Figure 5C–E). In addition, similar results were also observed in the *KP* tumor-derived L574 cells (Figure 5). These results suggest that CBX4 acts as an oncogenic driver in both human and mouse LUAD cells.

CBX4 facilitates growth of LUAD cells through the Wnt/β-catenin pathway

Previous study reported that CBX4 promotes tumor growth through increasing transcriptional activity of HIF-1α to enhance tumor angiogenesis in hepatocellular carcinoma [27]. To assess whether CBX4 facilitates LUAD development via promoting tumor angiogenesis, we evaluated the expression of VEGF in tumors from *KP* and *KPC* mice. Though increased expression of VEGF was noted in tumors from *KP* and *KPC* mice when compared to *WT* mice, no major changes in expression levels of VEGF or VEGFR2 were observed between tumors from *KP* and *KPC* mice (Figure S2), indicative of other mechanism.

The Wnt/β-catenin pathway has been implicated in the pathogenesis of various types of cancers including LUAD [40–44]. Interestingly, we found that protein levels of β-catenin were greatly reduced in the tumors from *KPC* mice vs *KP* mice (Figure 6A), indicating that the Wnt/β-catenin pathway might be involved in mediating the CBX4's action. To test this hypothesis, we evaluated the levels of β-catenin and found that knockdown of CBX4 in A549 cells greatly reduced β-catenin expression at both RNA and protein levels (Figure 6B–D). In addition, the expression levels of the β-catenin
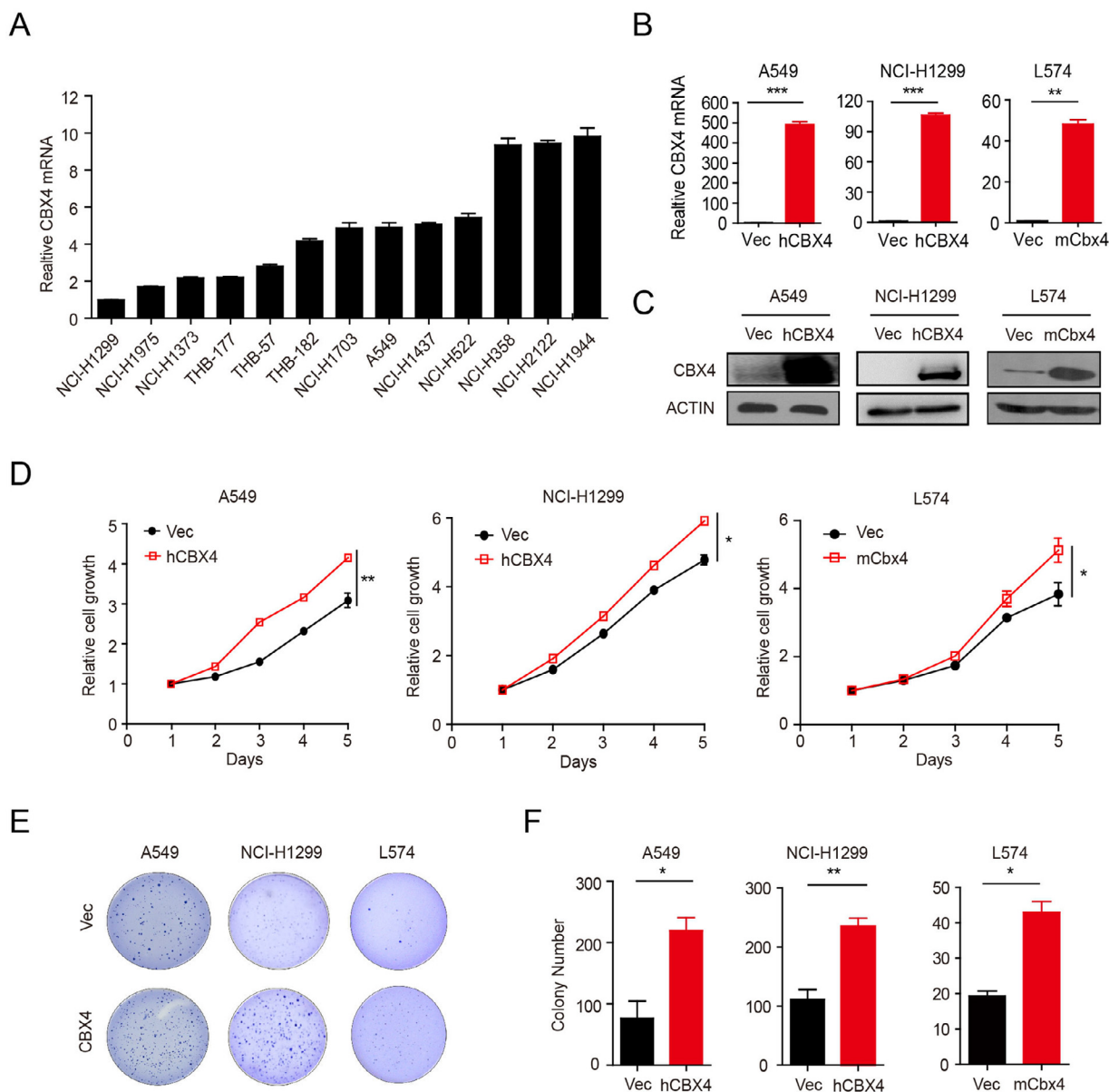
Fig. 4. Ectopic expression of CBX4 promotes proliferation and anchorage-independent growth in both human and mouse LUAD cells. (A) The expression of CBX4 in multiple human LUAD cell lines. (B and C) Real-time PCR (B) and western blot (C) analysis of A549, NCI-H1299, and L574 (*KP* mouse lung cancer cell line) cells with or without ectopic expression of CBX4. ACTIN or GAPDH is used as a loading control. (D) MTT analysis of cell proliferation in A549, NCI-H1299, and L574 cells with or without ectopic expression of CBX4. (E and F) Colony formation ability of A549, NCI-H1299, and L574 cells with or without ectopic expression of CBX4 was determined by soft agar assay. Data are shown as means ± SEM. *$P < 0.05$, **$P < 0.01$, ***$P < 0.001$.

downstream target genes, c-Myc and cyclinD1, were also down-regulated in CBX4-depleted cells (Figure 6B,C). Conversely, ectopic CBX4 expression clearly up-regulated the levels of β-catenin as well as its downstream targets c-Myc and cyclinD1 in A549 cells (Figure 6E–G). These results confirmed the positive regulation of β-catenin by CBX4. More important, knockdown of β-catenin through siRNA not only markedly inhibited the expression of β-catenin as well as its downstream targets c-Myc and cyclinD1 (Figure 6H–I), but also abrogated the effects of CBX4 on cell growth and colony formation in soft agar (Figure 6J–L). Furthermore, a positive correlation between the expression of CBX4 and β-catenin was also observed in human LUAD samples at both the RNA and protein levels (Figure 6M–O). Taken together, these data support the notion that CBX4 contributes to tumorigenesis of LUAD through activation of the Wnt/β-catenin pathway.

Discussion

PcG proteins are crucial epigenetic regulators that control multiple physiological processes including stem cell self-renewal, differentiation, and senescence. PcG proteins are identified in several families of protein complexes including PRC1 and PRC2. The recruitment of PRC1 to chromatin is thought to be mediated in part by the conserved chromodomain of CBX family proteins including CBX2, CBX4, CBX6, CBX7, and CBX8 [4–8]. Dysregulation of PcG proteins has been linked to tumorigenesis. Despite of structural similarities and functional redundancies, different members of CBX family were found to play distinct roles in a tissue type-dependent manner [4–8]. Up to now, the clinical relevance and biological function of CBX family proteins in lung cancer remain incompletely
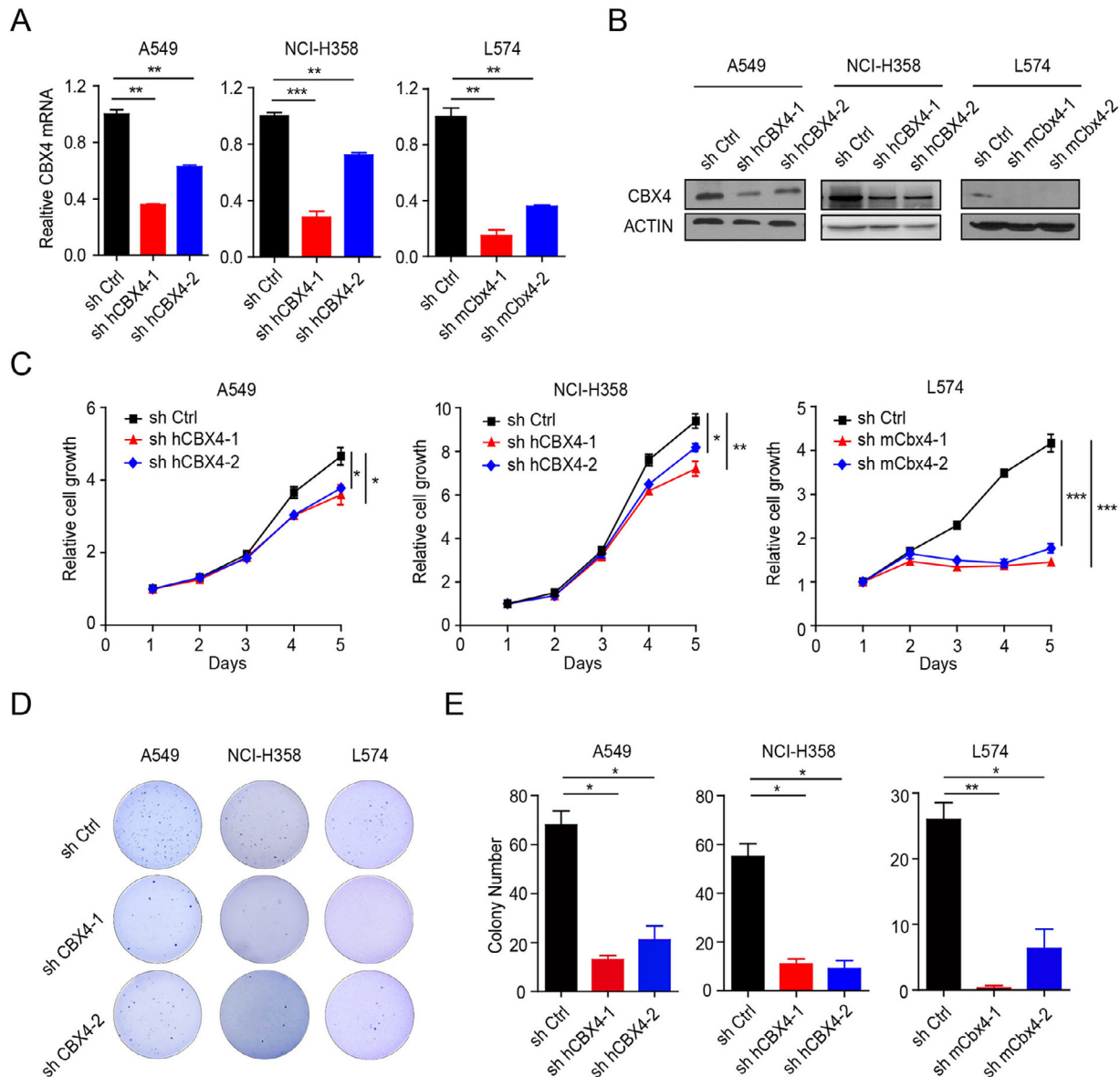
Fig. 5. Depletion of CBX4 impairs proliferation and anchorage-independent growth in both human and mouse LUAD cells. (A and B) Real-time PCR (A) and western blot (B) analysis of A549, NCI-H358, and L574 cells with or without CBX4 knockdown. (C) MTT analysis of cell proliferation in the A549, NCI-H358, and L574 cells with or without CBX4 knockdown. (D and E) Colony formation ability of the A549, NCI-H358, and L574 cells with or without CBX4 knockdown was determined by soft agar assay. Data are shown as means ± SEM. *$P < 0.05$, **$P < 0.01$, ***$P < 0.001$.

understood. In the present study, we find that CBX4 expression is frequently up-regulated in LUAD tissues and correlates with poor patient outcome. Through integrative analysis of LUAD GEMM, MEFs as well as human and mouse LUAD cell lines, we provide strong evidence to suggest an oncogenic activity for CBX4 in the tumorigenesis of LUAD. Moreover, our results reveal that CBX4 facilitates LUAD development via the Wnt/β-catenin pathway.

Aberrant expression and prognostic significance of CBX4 has been documented in several human malignancies including liver cancer, colorectal cancer, and breast cancer as well as lung cancer [27,29,45,46]. In fact, during the course of the present study, Hu et al independently reported the ability of CBX4 to promote the proliferation and metastasis in lung cancer [29]. Of note, the in vivo validation in their study was performed using xenografts of established human lung cancer cell lines in nude mice. Though tumor cell lines-based in vivo work is a valid approach, it also has some inherent limitations. The process of tumorigenesis could not be faithfully modelled

by subcutaneous injection of established cancer cell lines, probably due to the lack of its natural microenvironment and differences in growth kinetics of such tumors, which makes the cell line-based models less physiological relevant than autochthonous cancer models. In fact, GEMMs can more faithfully recapitulate histopathologic and molecular features of human disease and have a better predictive power for drug response [47,48]. Indeed, conflict results regarding gene functions in cancer between cell model-based and mouse model-based studies has been documented in literatures [49]. Thus, it is necessary and important to characterize the role of CBX4 in tumorigenesis using autochthonous GEMMs of LUAD. To address this, we employ the well-established *KP* mouse model and demonstrate that genetic ablation of Cbx4 profoundly attenuated lung tumor formation and improved survival in mice. These results not only are in accordance with Hu's study, but also provide direct in vivo evidence for CBX4 involvement in LUAD tumorigenesis.
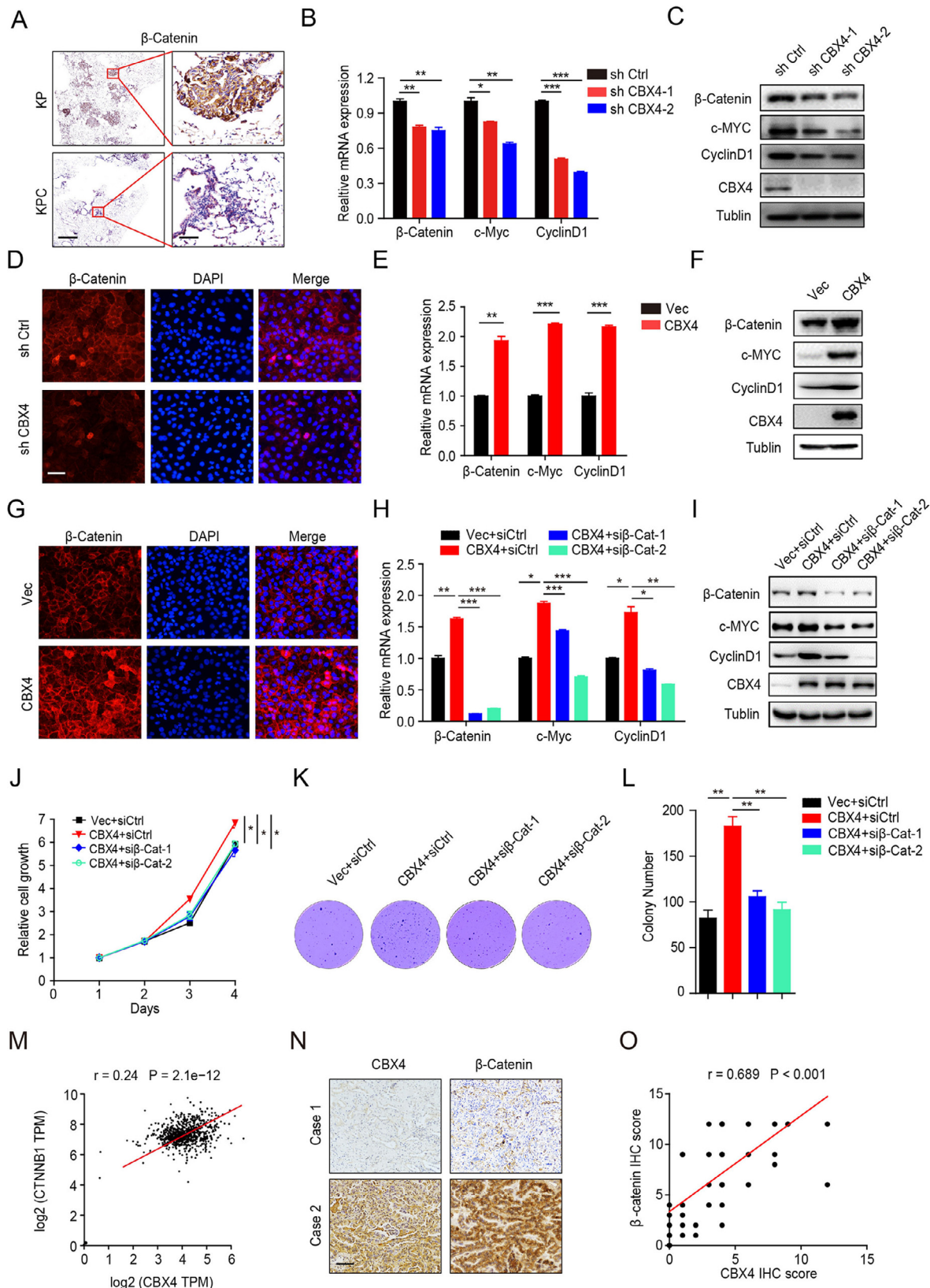
Similar to Hu's findings, we also observe the frequently up-regulation of CBX4 in human LUAD tissues. In addition, we find that CBX4 expression was also up-regulated in the lung tumors from *KP* mice, which is consistent with the results from clinical samples. We perform KRAS knockdown experiment and find that depletion of KRAS did not disturb the CBX4 expression in A549 cells (Figure S3). Besides, we did not observe an obvious up-regulation of CBX4 in tumors from Kras^{G12D} mice compared with adjacent normal tissues (Figure S4). These results indicate that mutant KRAS may not be responsible for the CBX4 up-regulation in *KP* mice. Future efforts will be needed to dissect the molecular basis for CBX4 up-regulation in LUAD. Moreover, we perform survival analysis and observe a significant association between increased CBX4 expression and poor patient survival both in our cohort and publicly available human LUAD datasets. Thus, our results indicate that increased CBX4 expression may predict worse prognosis of patients with LUAD. The unfavorable prognostic value of CBX4 in LUAD reported here are in accordance with previous observations in liver and breast cancers [27,46]. While we did not observe a correlation between CBX4 expression and survival of patients with LUSC, implying that this PRC1 core component may not be a prognostic indicator in LUSC. Whether CBX4 is also functionally important in LUSC requires future investigations.

To further determine the oncogenic activity of CBX4 in LUAD, we evaluate the effects of CBX4 ablation on growth and malignant transformation abilities of MEFs isolated from *KP* mice. The facts that CBX4 deficiency markedly inhibited anchorage-independent growth of *KP* MEFs in soft agar suggest that CBX4 is essential for the malignant transformation of *KP* MEFs. In agreement with the results from MEFs, our gain-of-function and loss-of-function experiments performed in different human and mouse LUAD cells consistently demonstrated an oncogenic activity of CBX4 in LUAD cells. All these in vivo and in vitro functional studies unambiguously support that CBX4 is an important regulator involved in LUAD initiation and development, which may at least partially explain the unfavorable prognostic significance of CBX4 in LUAD.

PRC1 has been shown to repress a number of nonlineage-specific transcription factors that directly affect β-catenin/Tcf transcriptional activity, by which preserves Wnt/β-catenin activity in adult stem cells to maintain intestinal homeostasis and supports tumor formation [50]. Interestingly, we find that depletion of CBX4 greatly suppressed the expression of β-catenin in *KP* mice. In addition, knockdown of CBX4 markedly inhibited β-catenin and its downstream targets c-Myc and cyclinD1 both at mRNA and protein levels, whereas ectopic expression of CBX4 did the opposite. More important, we demonstrate that knockdown of β-catenin efficiently blocked the oncogenic property of CBX4. Furthermore, we observe a positive correlation between CBX4 and β-catenin expression in human LUAD samples at both the mRNA and protein levels, which is in agreement with our in vivo and in vitro findings. In our system, we also observe that CBX4 could positively regulate BIM-1 expression, in line with the findings from Hu's study (data not shown). While to our knowledge, the current study is the

first to report the regulation of the Wnt/β-catenin pathway by CBX4. Given the complexity of mechanisms underlying LUAD tumorigenesis, we cannot rule out the potential involvement of other signaling cascades in this process. Nevertheless, our results highlight the functional importance of the Wnt/β-catenin pathway in mediating CBX4's action in LUAD. Further studies will be necessary to elucidate the mechanisms by which CBX4 activates the Wnt/β-catenin pathway.

CBX4 has been reported to have E3 SUMO-protein ligase activity that facilitates SUMO1 conjugation by UBE2I, and contributes to sumoylation of HNRNPK, a p53/TP53 transcriptional co-activator [51,52]. A recent study revealed that CBX4 has the ability to facilitate VEGF expression and promote angiogenesis in hepatocellular carcinoma through HIF-1α sumoylation, thereby enhancing its transcriptional activity [27]. While in this study, we did not observe a major change in VEGF or VEGFR2 expression between lung tumors from *KP* and *KPC* mice. And the levels of HIF-1α were not significantly changed either in CBX4-overexpressed or depleted A549 cells compared to controls (Figure S5), implying that the exact function of CBX4 in LUAD and in liver cancer may be different. In fact, CBX4 has been reported to act as a tumor suppressor in colorectal cancer [28]. Thus, the discrepant effects of CBX4 in different cancers indicate that its biological function is tissue-dependent and varies with the type of malignancy. Currently, it is unclear whether the observed effects of CBX4 on Wnt/β-catenin pathway as well as LUAD tumorigenesis is related to its E3 SUMO-protein ligase activity. More efforts should be warranted to dissect it into details in the future.

Conclusions

Here we provide direct in vivo evidence and in vitro validation highlighting the importance of CBX4 in the tumorigenesis of LUAD, which exerts its oncogenic activities via activation of the Wnt/β-catenin pathway and could serve as a potential therapeutic target in LUAD.

Author contributions

Hongbin Ji and Liang Hu conceived and supervised the study. Zuoyun Wang designed the study, performed the experiments, and analyzed the data. Zuoyun Wang, Liang Hu, and Hongbin Ji wrote the manuscript. Zhaoyuan Fang did the bioinformatics analysis. Gaobin Chen, Bo Liu, Jinjin Xu, Fei Li, Fuming Li, XiangKun Han, Hongyan Liu, Haoen Zhang, Yihua Sun, Gang Tian, Haiquan Chen, Guoliang Xu, and Lei Zhang provided technical supports and helpful comments.

Conflict of interest

The authors declare no conflict of interest.

Fig. 6. CBX4 exerts oncogenic properties in LUAD cells through the Wnt/β-catenin pathway. Representative IHC staining of β-catenin in the lung tumors from *KP* and *KPC* mice. Scale bar: 500 μm (left); 50 μm (right). (B) Real-time PCR analysis of β-catenin and its downstream targets c-Myc and CyclinD1 in A549 with or without CBX4 knockdown. (C) Western blot analysis of β-catenin and its downstream targets c-Myc and CyclinD1 in A549 cells with or without CBX4 knockdown. (D) IF staining of β-catenin in A549 cells with or without CBX4 knockdown. Scale bar: 500 μm. (E) Real-time PCR analysis of β-catenin and its downstream targets c-Myc and CyclinD1 in A549 with or without CBX4 overexpression. (F) Western blot analysis of β-catenin and its downstream targets c-Myc and CyclinD1 in A549 cells with or without CBX4 overexpression. (G) IF staining of β-catenin in A549 with or without CBX4 overexpression. (H) Real-time PCR analysis of β-catenin and its downstream targets c-Myc and CyclinD1 in control or CBX4-overexpressed A549 cells treated with or without siβ-catenin. (I) Western blot analysis of β-catenin and its downstream targets c-Myc and CyclinD1 in control or CBX4-overexpressed A549 cells treated with or without siβ-catenin. (J) MTT analysis of cell proliferation in control or CBX4-overexpressed A549 cells treated with or without siβ-catenin. (K and L) Colony formation ability of control or CBX4-overexpressed A549 cells treated with or without siβ-catenin was determined by soft agar assay. (M) The correlation of CBX4 and CTNNB1 (β-catenin) expression in clinical LUAD samples using the TCGA-LUAD dataset. (N) Representative IHC staining of CBX4 and β-catenin in 2 human LUAD samples. Scale bar: 100 μm. (O) Spearman correlation analysis of CBX4 and β-catenin protein expression in the 72 human LUAD samples. Data are shown as means ± SEM. *$P < 0.05$, **$P < 0.01$, ***$P < 0.001$, ns means no significance.

Funding

Acknowledgments

Supplementary materials

Supplementary material associated with this article can be found, in the online version, at doi:10.1016/j.neo.2020.12.005.

References

1 Hanahan D, Weinberg RA. The hallmarks of cancer: the next generation. *Cell* 2011;**144**(1):646–74.

2 Bray F, Ferlay J, Soerjomataram I, Siegel RL, Torre LA, Jemal A. Global cancer statistics 2018: GLOBOCAN estimates of incidence and mortality worldwide for 36 cancers in 185 countries. *CA Cancer J Clin* 2018;**68**(6):394–424.

3 Reck M, Heigener DF, Mok T, Soria JC, Rabe KF. Management of non-small-cell lung cancer: recent developments. *Lancet* 2013;**382**(9893):709–19.

4 Klauke K, Radulovic V, Broekhuis M, Weersing E, Zwart E, Olthof S, Ritsema M, Bruggeman S, Wu X, Helin K, Bystrykh L, et al. Polycomb Cbx family members mediate the balance between haematopoietic stem cell self-renewal and differentiation. *Nat Cell Biol* 2013;**15**(4):353–62.

5 Morey L, Pascual G, Cozzuto L, Roma G, Wutz A, Benitah SA, Di Croce L. Nonoverlapping functions of the Polycomb group Cbx family of proteins in embryonic stem cells. *Cell Stem Cell* 2012;**10**(1):47–62.

6 Ren X, Hu B, Song M, Ding Z, Dang Y, Liu Z, Zhang W, Ji Q, Ren R, Ding J, et al. Maintenance of Nucleolar Homeostasis by CBX4 Alleviates Senescence and Osteoarthritis. *Cell Rep* 2019;**26**(13) 3643-56 e7.

7 Lin YW, Chen HM, Fang JY. Gene silencing by the Polycomb group proteins and associations with cancer. *Cancer Invest* 2011;**29**(3):187–95.

8 Richly H, Aloia L, Di Croce L. Roles of the Polycomb group proteins in stem cells and cancer. *Cell Death Dis* 2011;**2**:e204.

9 Dawson MA, Kouzarides T. Cancer epigenetics: from mechanism to therapy. *Cell* 2012;**150**(1):12–27.

10 Fillmore CM, Xu C, Desai PT, Berry JM, Rowbotham SP, Lin YJ, Zhang H, Marquez VE, Hammerman PS, Wong KK, et al. EZH2 inhibition sensitizes BRG1 and EGFR mutant lung tumours to TopoII inhibitors. *Nature* 2015;**520**(7546):239–42.

11 Chase A, Cross NC. Aberrations of EZH2 in cancer. *Clin Cancer Res* 2011;**17**(9):2613–18.

12 Chen Y, Xie D, Yin Li W, Man Cheung C, Yao H, Chan CY, Xu FP, Liu YH, Sung JJ, et al. RNAi targeting EZH2 inhibits tumor growth and liver metastasis of pancreatic cancer in vivo. *Cancer Lett* 2010;**297**(1):109–16.

13 Varambally S, Dhanasekaran SM, Zhou M, Barrette TR, Kumar-Sinha C, Sanda MG, Ghosh D, Pienta KJ, Sewalt RG, Otte AP, et al. The polycomb group protein EZH2 is involved in progression of prostate cancer. *Nature* 2002;**419**(6907):624–9.

14 Yu J, Cao Q, Yu J, Wu L, Dallol A, Li J, Chen G, Grasso C, Cao X, Lonigro RJ, et al. The neuronal repellent SLIT2 is a target for repression by EZH2 in prostate cancer. *Oncogene* 2010;**29**(39):5370–80.

15 Zhang H, Qi J, Reyes JM, Li L, Rao PK, Li F, et al. Oncogenic Deregulation of EZH2 as an Opportunity for Targeted Therapy in Lung Cancer. *Cancer Discov* 2016;**6**(9):1006–21.

16 Mahmoudi T, Verrijzer CP. Chromatin silencing and activation by Polycomb and trithorax group proteins. *Oncogene* 2001;**20**(24):3055–66.

17 Vincenz C, Kerppola TK. Different polycomb group CBX family proteins associate with distinct regions of chromatin using nonhomologous protein sequences. *Proc Natl Acad Sci U S A* 2008;**105**(43):16572–7.

18 Wheeler LJ, Watson ZL, Qamar L, Yamamoto TM, Post MD, Berning AA, Spillman MA, Behbakht K, Bitler BG. CBX2 identified as driver of anoikis escape and dissemination in high grade serous ovarian cancer. *Oncogenesis* 2018;**7**(11):92.

19 Clermont PL, Sun L, Crea F, Thu KL, Zhang A, Parolia A, Lam WL, Helgason CD. Genotranscriptomic meta-analysis of the Polycomb gene CBX2 in human cancers: initial evidence of an oncogenic role. *Br J Cancer* 2014;**111**(8):1663–72.

20 Bernard D, Martinez-Leal JF, Rizzo S, Martinez D, Hudson D, Visakorpi T, Peters G, Carnero A, Beach D, Gil J. CBX7 controls the growth of normal and tumor-derived prostate cells by repressing the Ink4a/Arf locus. *Oncogene* 2005;**24**(36):5543–51.

21 Forzati F, Federico A, Pallante P, Abbate A, Esposito F, Malapelle U, Sepe R, Palma G, Troncone G, Scarfo M, Arra C, et al. CBX7 is a tumor suppressor in mice and humans. *J Clin Invest* 2012;**122**(2):612–23.

22 Scott CL, Gil J, Hernando E, Teruya-Feldstein J, Narita M, Martinez D, Visakorpi T, Mu D, Cordon-Cardo C, Peters G, et al. Role of the chromobox protein CBX7 in lymphomagenesis. *Proc Natl Acad Sci U S A* 2007;**104**(13):5389–94.

23 Lee SH, Um SJ, Kim EJ. CBX8 suppresses Sirtinol-induced premature senescence in human breast cancer cells via cooperation with SIRT1. *Cancer Lett* 2013;**335**(2):397–403.

24 Song X, Tang T, Li C, Liu X, Zhou L. CBX8 and CD96 Are Important Prognostic Biomarkers of Colorectal Cancer. *Med Sci Monit* 2018;**24**:7820–7.

25 Pallante P, Forzati F, Federico A, Arra C, Fusco A. Polycomb protein family member CBX7 plays a critical role in cancer progression. *Am J Cancer Res* 2015;**5**(5):1594–601.

26 Li B, Zhou J, Liu P, Hu J, Jin H, Shimono Y, Takahashi M, Xu G. Polycomb protein Cbx4 promotes SUMO modification of de novo DNA methyltransferase Dnmt3a. *Biochem J* 2007;**405**(2):369–78.

27 Li J, Xu Y, Long XD, Wang W, Jiao HK, Mei Z, Yin QQ, Ma LN, Zhou AW, Wang LS, et al. Cbx4 governs HIF-1alpha to potentiate angiogenesis of hepatocellular carcinoma by its SUMO E3 ligase activity. *Cancer Cell* 2014;**25**(1):118–31.

28 Wang X, Li L, Wu Y, Zhang R, Zhang M, Liao D, Wang G, Qin G, Xu RH, Kang T. CBX4 Suppresses Metastasis via Recruitment of HDAC3 to the Runx2 Promoter in Colorectal Carcinoma. *Cancer Res* 2016;**76**(24):7277–89.

29 Hu C, Zhang Q, Tang Q, Zhou H, Liu W, Huang J, Liu Y, Wang Q, Zhang J, Zhou M, et al. CBX4 promotes the proliferation and metastasis via regulating BMI-1 in lung cancer. *J Cell Mol Med* 2020;**24**(1):618–31.

30 Liu B, Liu YF, Du YR, Mardaryev AN, Yang W, Chen H, Xu ZM, Xu CQ, Zhang XR, Botchkarev VA, et al. Cbx4 regulates the proliferation of thymic epithelial cells and thymus function. *Development* 2013;**140**(4):780–8.

31 Wang Z, Feng Y, Bardeesy N, Wong KK, Liu XY, Ji H. Temporal dissection of K-ras(G12D) mutant in vitro and in vivo using a regulatable K-ras(G12D) mouse allele. *PLoS One* 2012;**7**(5):e37308.

32 Tang L, Tan YX, Jiang BG, Pan YF, Li SX, Yang GZ, Wang M, Wang Q, Zhang J, Zhou WP, et al. The prognostic significance and therapeutic potential

of hedgehog signaling in intrahepatic cholangiocellular carcinoma. *Clin Cancer Res* 2013;**19**(8):2014–24.

33 Wang Z, Sun Y, Gao B, Lu Y, Fang R, Gao Y, Xiao T, Liu XY, Pao W, Zhao Y, et al. Two co-existing germline mutations P53 V157D and PMS2 R20Q promote tumorigenesis in a familial cancer syndrome. *Cancer Lett* 2014;**342**(1):36–42.

34 Han CP, Kok LF, Wang PH, Wu TS, Tyan YS, Cheng YW, Lee MY, Yang SF. Scoring of p16(INK4a) immunohistochemistry based on independent nuclear staining alone can sufficiently distinguish between endocervical and endometrial adenocarcinomas in a tissue microarray study. Modern pathology: an official journal of the United States and Canadian Academy of Pathology. *Inc* 2009;**22**(6):797–806.

35 Gyorffy B, Surowiak P, Budczies J, Lanczky A. Online survival analysis software to assess the prognostic value of biomarkers using transcriptomic data in non-small-cell lung cancer. *PLoS One* 2013;**8**(12):e82241.

36 DuPage M, Dooley AL, Jacks T. Conditional mouse lung cancer models using adenoviral or lentiviral delivery of Cre recombinase. *Nat Protoc* 2009;**4**(7):1064–72.

37 Li F, Han X, Li F, Wang R, Wang H, Gao Y, Wang X, Fang Z, Zhang W, Yao S, et al. LKB1 Inactivation Elicits a Redox Imbalance to Modulate Non-small Cell Lung Cancer Plasticity and Therapeutic Response. *Cancer Cell* 2015;**27**(5):698–711.

38 Prieto I, Zambrano A, Laso J, Aranda A, Samper E, Monsalve M. Early induction of senescence and immortalization in PGC-1alpha-deficient mouse embryonic fibroblasts. *Free Radic Biol Med* 2019;**138**:23–32.

39 Yao S, Huang HY, Han X, Ye Y, Qin Z, Zhao G, Li F, Hu G, Hu L, Keratin Ji H. 14-high subpopulation mediates lung cancer metastasis potentially through Gkn1 upregulation. *Oncogene* 2019;**38**(36):6354–69.

40 Bafico A, Liu G, Goldin L, Harris V, Aaronson SA. An autocrine mechanism for constitutive Wnt pathway activation in human cancer cells. *Cancer Cell* 2004;**6**(5):497–506.

41 Uematsu K, He B, You L, Xu Z, McCormick F, Jablons DM. Activation of the Wnt pathway in non small cell lung cancer: evidence of dishevelled overexpression. *Oncogene* 2003;**22**(46):7218–21.

42 Uren A, Fallen S, Yuan H, Usubutun A, Kucukali T, Schlegel R, Toretsky JA. Activation of the canonical Wnt pathway during genital keratinocyte transformation: a model for cervical cancer progression. *Cancer Res* 2005;**65**(14):6199–206.

43 Lemieux E, Cagnol S, Beaudry K, Carrier J, Rivard N. Oncogenic KRAS signalling promotes the Wnt/beta-catenin pathway through LRP6 in colorectal cancer. *Oncogene* 2015;**34**(38):4914–27.

44 Wang L, Heidt DG, Lee CJ, Yang H, Logsdon CD, Zhang L, Fearon ER, Ljungman M, Simeone DM. Oncogenic function of ATDC in pancreatic cancer through Wnt pathway activation and beta-catenin stabilization. *Cancer Cell* 2009;**15**(3):207–19.

45 Wang X, Kang T. Role of CBX4 in the Colorectal Carcinoma Metastasis-Response. *Cancer Res* 2017;**77**(9):2550–1.

46 Zeng JS, Zhang ZD, Pei L, Bai ZZ, Yang Y, Yang H, Tian QH. CBX4 exhibits oncogenic activities in breast cancer via Notch1 signaling. *Int J Biochem Cell Biol* 2018;**95**:1–8.

47 Singh M, Murriel CL, Johnson L. Genetically engineered mouse models: closing the gap between preclinical data and trial outcomes. *Cancer Res* 2012;**72**(11):2695–700.

48 Kersten K, de Visser KE, van Miltenburg MH, Jonkers J. Genetically engineered mouse models in oncology research and cancer medicine. *EMBO Mol Med* 2017;**9**(2):137–53.

49 Moroishi T, Hayashi T, Pan WW, Fujita Y, Holt MV, Qin J, Carson DA, Guan KL. The Hippo Pathway Kinases LATS1/2 Suppress Cancer Immunity. *Cell* 2016;**167**(6) 1525-1539 e17.

50 Chiacchiera F, Rossi A, Jammula S, Piunti A, Scelfo A, Ordonez-Moran P, Koseki H, Pasini D. Polycomb Complex PRC1 Preserves Intestinal Stem Cell Identity by Sustaining Wnt/beta-Catenin Transcriptional Activity. *Cell Stem Cell* 2016;**18**(1):91–103.

51 Kagey MH, Melhuish TA, Wotton D. The polycomb protein Pc2 is a SUMO E3. *Cell* 2003;**113**(1):127–37.

52 Pelisch F, Pozzi B, Risso G, Munoz MJ, Srebrow A. DNA damage-induced heterogeneous nuclear ribonucleoprotein K sumoylation regulates p53 transcriptional activation. *J Biol Chem* 2012;**287**(36):30789–99.